Biochemical and Biophysical Research Communications 444 (2014) 311–318

Contents lists available at ScienceDirect

Biochemical and Biophysical Research Communications

journal homepage: www.elsevier.com/locate/ybbrc

Modeling of Menkes disease via human induced pluripotent stem cells

Ji-Hoon Suh [a], Dongkyu Kim [b], Hyemin Kim [b,1], David M. Helfman [b], Jin-Ho Choi [c], Beom Hee Lee [c], Han-Wook Yoo [c], Yong-Mahn Han [a,b,*]

[a] Graduate Schools of Medical Science and Engineering, KAIST, 291 Daehak-ro, Yuseong-gu, Daejeon 305-701, Republic of Korea
[b] Department of Biological Sciences, KAIST, 291 Daehak-ro, Yuseong-gu, Daejeon 305-701, Republic of Korea
[c] Department of Pediatrics, Asan Medical Center Children's Hospital, University of Ulsan College of Medicine, Seoul, Republic of Korea

ARTICLE INFO

Article history:
Received 24 December 2013
Available online 24 January 2014

Keywords:
Induced pluripotent stem cells
Cadherin
Neruonal
Menkes

ABSTRACT

Menkes disease (MD) is a copper-deficient neurodegenerative disorder that manifests severe neurologic symptoms such as seizures, lethargic states, and hypotonia. Menkes disease is due to a dysfunction of ATP7A, but the pathophysiology of neurologic manifestation is poorly understood during embryonic development. To understand the pathophysiology of neurologic symptoms, molecular and cellular phenotypes were investigated in Menkes disease-derived induced pluripotent stem cells (MD-iPSCs). MD-iPSCs were generated from fibroblasts of a Menkes disease patient. Abnormal reticular distribution of ATP7A was observed in MD-fibroblasts and MD-iPSCs, respectively. MD-iPSCs showed abnormal morphology in appearance during embryoid body (EB) formation as compared with wild type (WT)-iPSCs. Intriguingly, aberrant switch of E-cadherin (E-cad) to N-cadherin (N-cad) and impaired neural rosette formation were shown in MD-iPSCs during early differentiation. When extracellular copper was chelated in WT-iPSCs by treatment with bathocuprione sulfate, aberrant switch of E-cad to N-cad and impaired neuronal differentiation were observed, like in MD-iPSCs. Our results suggest that neurological defects in Menkes disease patients may be responsible for aberrant cadherin transition and impaired neuronal differentiation during early developmental stage.

1. Introduction

Menkes disease (MD) is characterized as an inherited form of copper deficiency [1,2]. For this reason, Menkes disease has been studied for the past three decades as a disease model to understand the role of copper in the human nervous system [3]. Menkes disease is an infantile-onset X-linked recessive neurodegenerative disorder caused by dysfunction of a copper-transporting ATPase, ATP7A [4–6]. ATP7A dysfunction results in diminished copper uptake, thereby leading to a copper deficient state in a patient's body [7,8]. The clinical manifestation of Menkes disease reflects decreased activities of enzymes that require copper as a cofactor, including dopamine-β-hydroxylase, cytochrome c oxydase, and peptidylglycine-α-amidating monooxygenase [9]. Among a wide spectrum of clinical manifestations caused by dysfunction of copper-requiring enzymes, neurologic symptoms are closely related with mortality and morbidity in Menkes disease patients. Infants born with Menkes disease begin to exhibit failure to thrive and developmental delay within several months after birth. Affected infants gradually manifest neurologic impairments (e.g. hypotonia, lethargic states and seizures), and usually die within 3 years of birth [10]. Treatment of choice, intravenous copper histidine injection, has shown to reduce the seizure susceptibility and hypertonicity in some patients [11,12]. However, even under ideal circumstance, Menkes disease infants treated with copper histidine exhibits suboptimal clinical outcomes [10]. To understand the pathophysiology of Menkes disease, ATP7A knockout mouse models have been used [13–15]. ATP7A knockout mice showed deficiency of olfactory sensory neuronal maturation during early neuronal development [13]. Expression of genes involving myelination, energy metabolism and translation was downregulated in cerebral cortex and cerebellum tissues of a Menkes disease patient [16]. Despite various pathologies in neuronal tissues in knockout mice and human cadavers, how the copper-deficient environment caused by ATP7A mutation affects neurologic manifestation in Menkes disease patients is poorly understood. Recently, it has been reported that human induced pluripotent stem cells (iPSCs) are useful systems to study mechanisms on human diseases during early development in organogenesis because of their differentiation capability into diverse cell types [17,18]. Here, we found that MD-iPSCs exhibited an aberrant switch of E-cad to N-cad and abnormal neural rosette formation during early differentiation.

* Corresponding author at: Department of Biological Sciences, KAIST, 291 Daehak-ro, Yuseong-gu, Daejeon 305-701, Republic of Korea. Fax: +82 42 350 8160.
E-mail address: ymhan@kaist.ac.kr (Y.-M. Han).
[1] Present address: Alternative Toxicological Methods Research Center, Korea Institute of Toxicology, 141 Gajeong-ro, Yuseong-gu, Daejeon 305-343, Republic of Korea.

0006-291X/$ - see front matter © 2014 Elsevier Inc. All rights reserved.
http://dx.doi.org/10.1016/j.bbrc.2014.01.038

Furthermore, MD-iPSCs were impaired in the structural integrity, including membrane recruitment and microdetachment, in the cell to cell junction. Knockdown of ATP7A expression did mimic cellular phenotypes of MD-iPSCs. Our findings demonstrate molecular and cellular aberrancies in MD-iPSCs. This study provides novel insights for understanding neurological pathophysiology in Menkes disease.

2. Materials and methods

2.1. Clinical history of a Menkes disease patient

We obtained fibroblasts from a 5 year old boy that was diagnosed as Menkes disease at 4 months after birth. Menkes disease patient's fibroblasts were obtained from Asan Medical Center under a protocol approved by the institutional review board. The patient had severe neurologic symptoms such as lethargic state and seizure (Table 1). Detailed clinical data were previously published [19]. He had a defective *ATP7A* gene in which G was changed to A on 4005th nucleotide of cDNA sequence (Fig. 1A).

2.2. Generation of induced pluripotent stem cells (iPSC) from a Menkes disease patient

Human iPSCs were generated from human skim fibroblasts (CRL-2097) and dermal fibroblasts of a Menkes disease patient by ectopic expression of OCT4, SOX2, KLF4, and C-MYC as previously described [20]. They were maintained on Mitomycin C (Sigma–Aldrich, St. Louis, MO)-treated mouse embryonic fibroblasts in the ESC medium at 37 °C. The embryonic stem cell medium consisted of DMEM-F12 (Invitrogen, Carlsbad, CA) supplemented with 20% serum replacement (Invitrogen), 1% NEAA (Invitrogen), 1% Penicillin–streptomycin (Invitrogen), 0.1 mM 2-mercaptoethanol (Sigma–Aldrich), and 4 ng/ml bFGF (Invitrogen).

2.3. Embryoid body (EB) formation and neuronal differentiation

Human iPSC colonies were divided into small pieces of approximately 5.5 mm × 5.5 mm squares by using McIlwain tissue chopper (Mickle Engineering, Westbury, NY), and then treated with 10 mg/ml dispase (Invitrogen) for 5 min to detach. Detached clumps were cultured in bFGF-free embryonic stem cell medium containing 10% SR for 7 days. Suspended EBs were attached on Matrigel™ (BD Bioscience, Bedford, MA)-coated dishes and then cultured in the same medium for 7 days. For neural rosette formation, spontaneous differentiation and directed neuronal differentiation were used as depicted in Supplementary data 3. For spontaneous differentiation, EBs were cultured for 7 days and attached on Matrigel-coated dishes. Attached EBs were cultured in the same medium for 7 days. For directed differentiation, we cultured EBs for 4–5 days and attached to Matrigel-coated dishes. Then, the cells were cultured in neuronal differentiation medium (DMEM/F12 + 20 ng/ml bFGF + N2 supplement) for 5–7 days.

Table 1
Clinical and molecular datas from Menkes disease with ATP7A mutation.

Family data	Age	5 years
	Sex	M
Clinical data	Initial onset	4 months
	CNS	Seizure, lethargic state
	NM	Hypotonia
	Other	Brittle hair
Genetic data	Nucleotide chages	c4005 + G > A
	Protein alteration	Exon 20 skipping

NM = neuromuscular.

2.4. RNA isolation and real time PCR analysis

Total RNAs were extracted from cells using the TRIzol Reagent (Invitrogen), and reverse-transcribed using M-MLV Reverse Transcriptase (Enzynomics, Daejeon, Korea) according to the manufacturer's protocol. Relative expression levels of genes were measured by real-time RT-PCR using 2× Prime Q-Master Mix (GENET BIO, Seoul, Korea) and analyzed with an iCycler iQ5 Real-Time detection system (Bio-Rad Laboratories, Hercules, CA). The primers used are listed in Supplementary Table 1. The reaction parameters for real-time RT-PCR were 95 °C for 10 min followed by 40 cycles of 95 °C for 30 s, 60 °C for 30 s, and 72 °C for 30 s, and a final elongation step at 72 °C for 5 min. For comparative analyses, mRNA expression levels were normalized to *GAPDH* and then expressed as fold-change. The sample ΔCt (SΔCt) value was calculated from the difference between the Ct values of *GAPDH* and the target genes. The relative gene expression levels between the sample and control were determined using the formula $2^{-(S\Delta Ct - C\Delta Ct)}$.

2.5. Immunocytochemistry

Cells were grown on a 4-well cell culture slide (SPL lifescience, South Korea), fixed with 4% formaldehyde at 4 °C for 30 min, permeabilized with 0.1% triton X-100 in PBS, and blocked with 4% normal donkey serum (Cell Signaling Technologies, Beverly, MA) or 3% BSA (Sigma–Aldrich) for 1 h at room temperature (RT). Subsequently, antibodies against E-cadherin (1:100), N-cadherin (1:100), NESTIN (1:200), SOX2 (1:200), TUJ-1 (1:200), MAP2 (1:200) were incubated with the prepared cells at 4 °C overnight. Finally, cells were washed several times with PBST (0.1% Tween-20 in PBS) and incubated with Alexa Fluor 488- or cy3-conjugated secondary antibodies (Invitrogen). Fluorescence was analyzed using fluorescence microscope (Olympus, Japan) or a Zeiss LSM 510 confocal microscope (Carl Zeiss, Germany). Number of N cadherin$^+$/Sox2$^+$ neural rosettes were counted per each well and statistically analyzed by a Mann–Whitney test.

2.6. Western blot analysis

Harvested cells were re-suspended in EBC lysis buffer (50 mM Tris–HCL8.0, 300 mM NaCl, 0.5% NP40) containing 100 μg/ml lysozyme, 10 μg/ml aprotininm and 10 μg/ml leupeptin. (Sigma–Aldrich). The cells in suspension were lysed by three–five cycles of sonication for 1 s on ice. After sonication, lysates were centrifuged at 16,100×*g* for 5 min at 4 °C. Protein concentration was determined by using Brad-ford assay. All sample preparations were diluted in 1× SDS loading buffer (60 mM Tris–HCl pH 6.8, 25% glycerol, 2% SDS, 14.4 mM β-mercaptoethanol, 0.1% bromphenol blue) and boiled for 2–3 min. Proteins were separated on 10% SDS–PAGE gel, high molecular weight protein (over 100 kDa) were separated on 6% SDS–PAGE gel respectively, and then transferred to the nitrocellulose membrane. After blocking with 4% of skim milk or 5% BSA, membranes were incubated with antibodies at 4 °C overnight, respectively. After washing with TBST, membranes were incubated with horseradish peroxidase-conjugated second antibodies in TBST containing 4% skim milk for 1 h. Quantitative Imaging of blots by ECL chemi-luminescence was detected with Fujifilm LAS4000 CCD camera system (Fugifilm, Japan).

2.7. Antibodies and reagent

Primary antibodies used in this study were anti-vimentin rat Ab (R&D systems); anti-E-cadherin mouse Ab and anti-N-cadherin mouse Ab (BD Transduction Laboratories, Lexington, KY); anti-Snail and anti-slug rabbit Ab and anti-SOX2 rabbit Ab (Cell Signaling Technologies); anti-Nestin mouse Ab (Chemicon, Temecula,

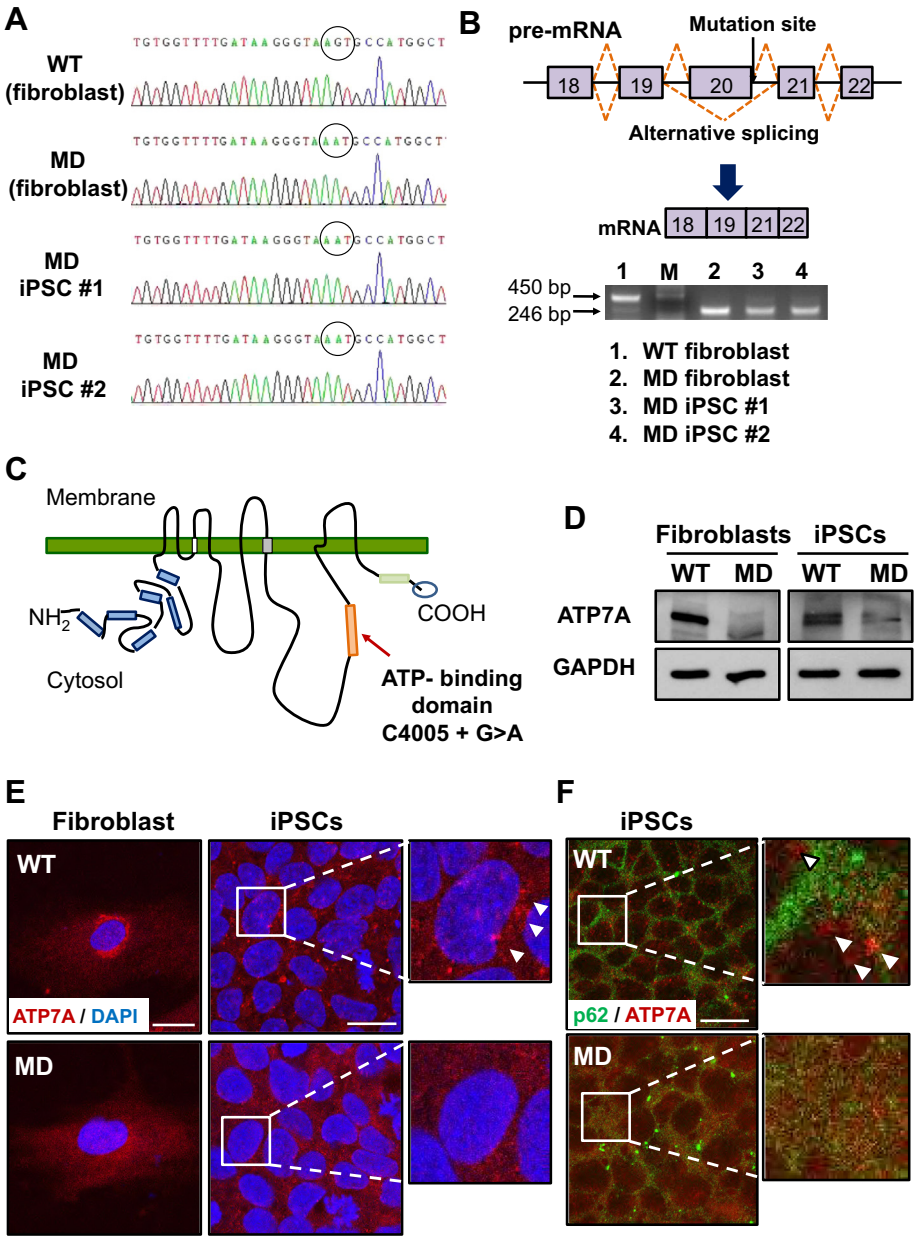

Fig. 1. Genetic information and localization of ATP7A in MD-iPSCs. (A) Genetic mutation of *ATP7A* gene. This gene shows single nucleotide change (c4005 + G > A) in MD-fibroblast and iPSCs. (B) Alternative splicing of mutated *ATP7A* gene. PCR products were shortened in MD-derivatives because exon 20 was skipped. (C) Schematic figure of mutation site. (D) Western blot of ATP7A in fibroblasts and iPSCs. (E) Localization of ATP7A in fibroblast and iPSCs. ATP7A proteins (red) were normally localized in perinuclear regions, but evenly dispersed in the cytoplasm in MD-iPSCs. White squares are magnified figures. White arrowheads show puncta forms of ATP7A protein in WT-iPSCs. (F) Immunostaining of ER (endoplasmic reticular) marker p62 (green) and ATP7A (red) in iPSCs. White squares are magnified figures. White arrowheads indicate ATP7A molecules localized apart from p62 in WT iPSCs. All scale bars represent 200 μm. (For interpretation of the references to color in this figure legend, the reader is referred to the web version of this article.)

CA); anti-β III tubulin rabbit Ab (Abcam, Cambridge, MA). For E cadherin and N cadherin co-staining anti-E cadherin rat (Abcam) was used. For immunoblot of ATP7A, anti-ATPA mouse Ab (Abcam), for immunostaining of ATP7A localization, anti-ATP7A rabbit Ab (Hycult Biotechnology, Uden, Netherland) were used. Copper chelating agent, bathocuprione sulfate (BCS) was purchased from Sigma–Aldrich and dissolved according to the manufacturer's protocol.

2.8. Measurement of intracellular copper concentration

Total cell lysates of fibroblasts, iPSCs and iPSCs-derivatives were prepared in acid-washed plastic labware and digested in a mixture of 2 ml of 65% HNO3 (Ultrex, JT Baker), and 7 ml deionized water. Prepared samples were wet mineralized in a START D microwave oven (Milestone Inc., Monroe, CT, USA) for 4 h at 150 °C. Copper levels were then analyzed by inductively coupled plasma (ICP) mass spectrometry (Agilent Technologies, Waldbronn, Germany).

3. Results

3.1. Characterization of mutations of ATP7A in MD-iPSCs

Characterization and pluripotency of MD-iPSCs were analyzed (Supplementary data 1). MD-iPSCs had a typical morphology with normal karyotype and expressed ES-specific markers. Promoters of pluripotent genes such as *OCT4*, *REX1* and *NANOG* were epigenetically reprogrammed in MD-iPSCs like in hESCs. Furthermore,

Table 2
Copper concentrations in fibroblasts and iPSCs.

	WT (ppb)	Menkes disease (ppb)
Copper concentration in fibroblasts	23.7 ± 15.0	63.5 ± 8.9
Copper concentrations in iPSCs	11.0 ± 4.0	13.4 ± 1.9

ppb = parts per billion (ng of copper/mg of protein).

MD-iPSCs formed teratomas after subcutaneous injection into nude mice. MD-iPSCs and MD-fibroblasts showed missense mutation (Fig. 1A) resulting in skipping of exon 20 (Fig. 1B). Mutation site was located in ATP-binding domain (Fig. 1C). Cultured MD-fibroblasts showed a higher intracellular copper concentration than wild type (WT)-fibroblasts, whereas copper concentrations of MD-iPSCs were similar to that of WT-iPSCs (Table 2). Expression level of ATP7A was decreased in MD-fibroblasts and MD-iPSCs compared to the controls, respectively (Fig. 1D). ATP7A molecules were intensively located around the perinuclear region within trans-Golgi network (TGN) in WT-fibroblasts (Fig. 1E, left upper), whereas it was evenly dispersed in the cytoplasm in MD-fibroblasts (Fig. 1E, left lower). The distribution of ATP7A molecules in WT-iPSCs represented small puncta forms around nucleus whereas MD-iPSCs showed dispersed distribution in cytoplasm (Fig. 1E, right). To further analyze the intracellular localization of ATP7A molecules in iPSCs, ATP7A was co-immunostained with p62, an endoplasmic reticulum (ER) marker. ATP7A molecules were apart from ER in WT-iPSCs, but were evenly distributed in MD-iPSCs (Fig. 1F). Thus, MD-iPSCs represented abnormal reticular distribution of ATP7A.

3.2. Aberrant switch of E-cadherin to N-cadherin and neuronal differentiation in MD-iPSCs during EB formation

Next, formation of embryoid body (EB) was carried out in order to test the pluripotency of MD-iPSCs *in vitro*. Intriguingly, MD-iPSC-derived EBs showed more opaque and compact struc-

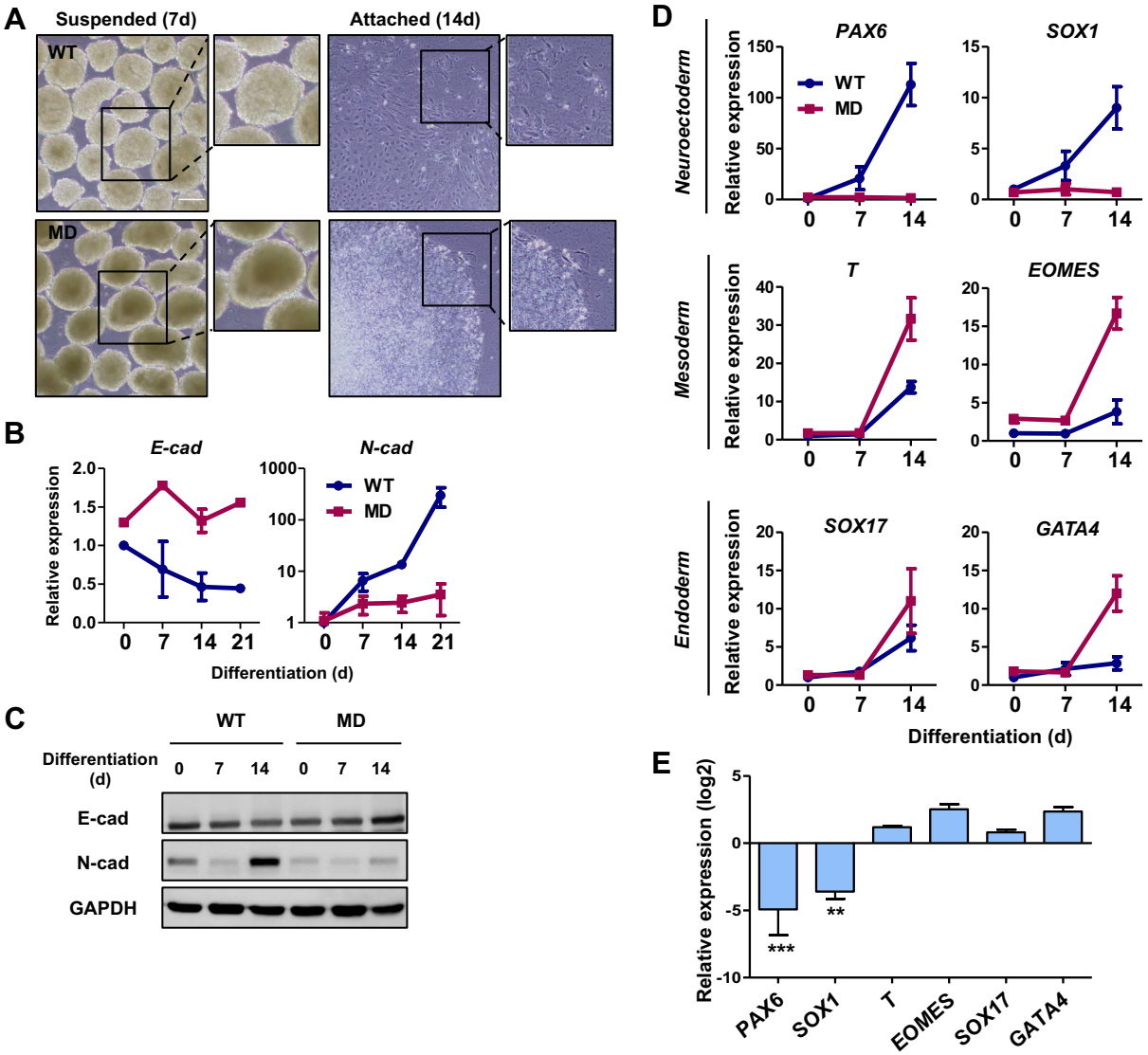

Fig. 2. Aberrant switch of E-cadherin to N-cadherin and impaired neuronal differentiation in MD-iPSCs during EB formation. (A) Phase-contrast images. WT- and MD-iPSCs formed EBs (left, day 7) and then further cultured on matrigel-coated dishes (right, day 14), respectively. Black squares show magnified images of each panel. Scale bar; 200 μm. (B) Quantitative transcription levels of *E-cad* and *N-cad* during early differentiation in WT- and MD-iPSCs. (C) Western blot analysis of E-cad and N-cad during early differentiation in WT- and MD-iPSCs. (D) Quantitative transcription levels of three lineage-specific genes (neuroectoderm, *PAX6* and *SOX1*; mesoderm, *T* and *EOMES*; endoderm, *SOX17* and *GATA4*) during early differentiation ($n = 3$). (E) Relative expression level of lineage-specific genes in MD-iPSC-derivatives compared with WT-iPSC-derivatives at 14 days of culture. p Values were analyzed by Mann–Whitney test ($^{***}p < 0.001$; $^{**}p < 0.01$).

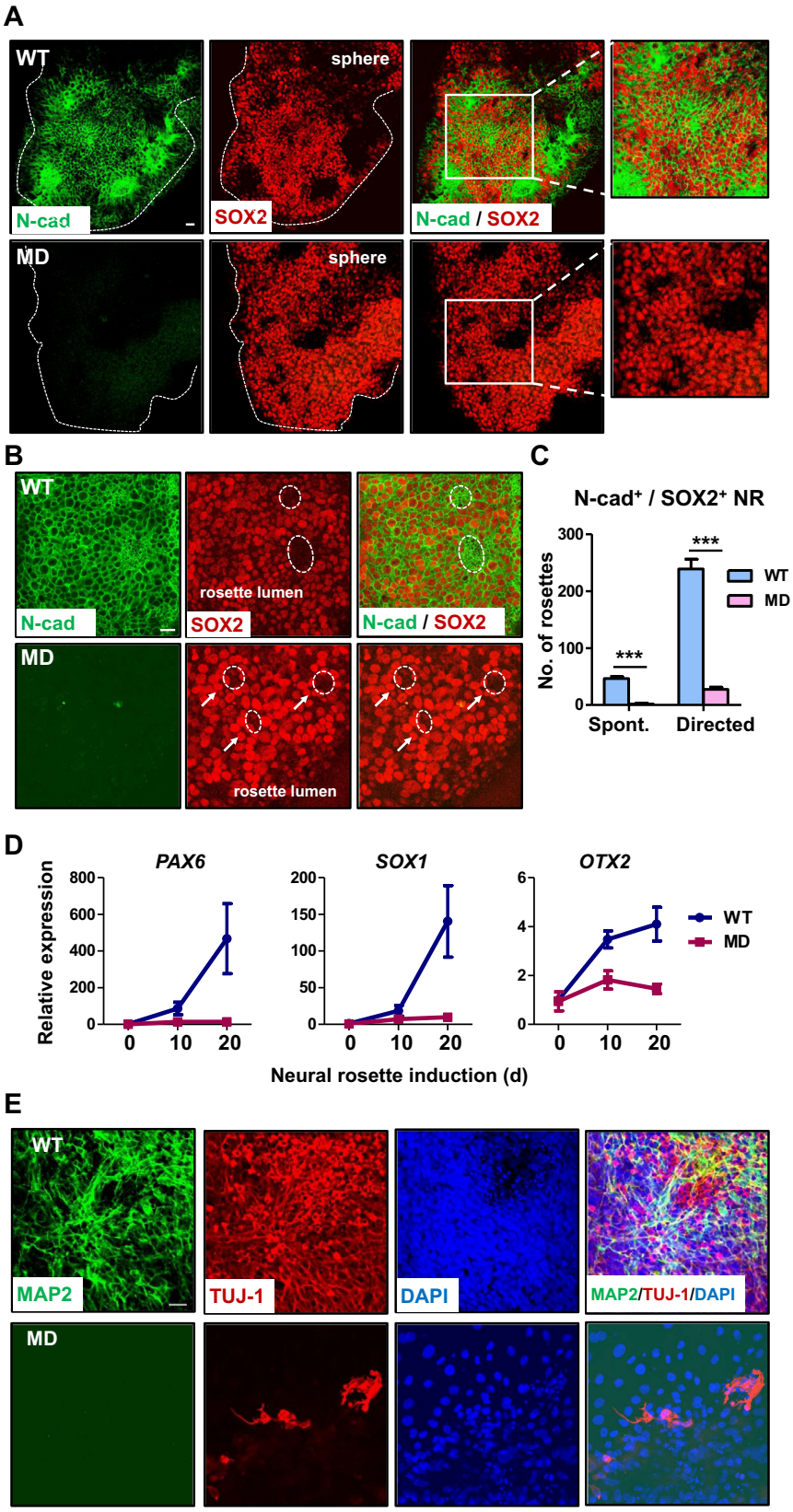

Fig. 3. A paucity of neural rosette formation in MD-iPSCs. (A) Immunostaining of N-cad (green) and SOX2 (red) in respective iPSCs-derived neurospheres by using spontaneous neuronal differentiation method. White dot lines represent margin of neurospheres. White squares are magnified images. (B) Immunostaining of N-cad (green) and SOX2 (red) by using directed neuronal differentiation method. White dot circles represent lumens of neural rosette structure. White arrows indicate empty lumens of rosette structures in MD-iPSC-derived neurospheres. (C) Number of N-cad/SOX2 double positive neural rosettes per each well. *p* Values were analyzed by Mann–Whitney test (***$p < 0.001$). (D) Quantitative transcription levels of early neuronal genes (*PAX6*, *SOX1* and *OTX2*) during neural rosette induction ($n = 4$). (E) Immunostaining of pan-neurite markers MAP2 (green), TUJ-1 (red) and DAPI (blue) in each neurosphere-derived neurite. All scale bars represent 200 μm. (For interpretation of the references to color in this figure legend, the reader is referred to the web version of this article.)

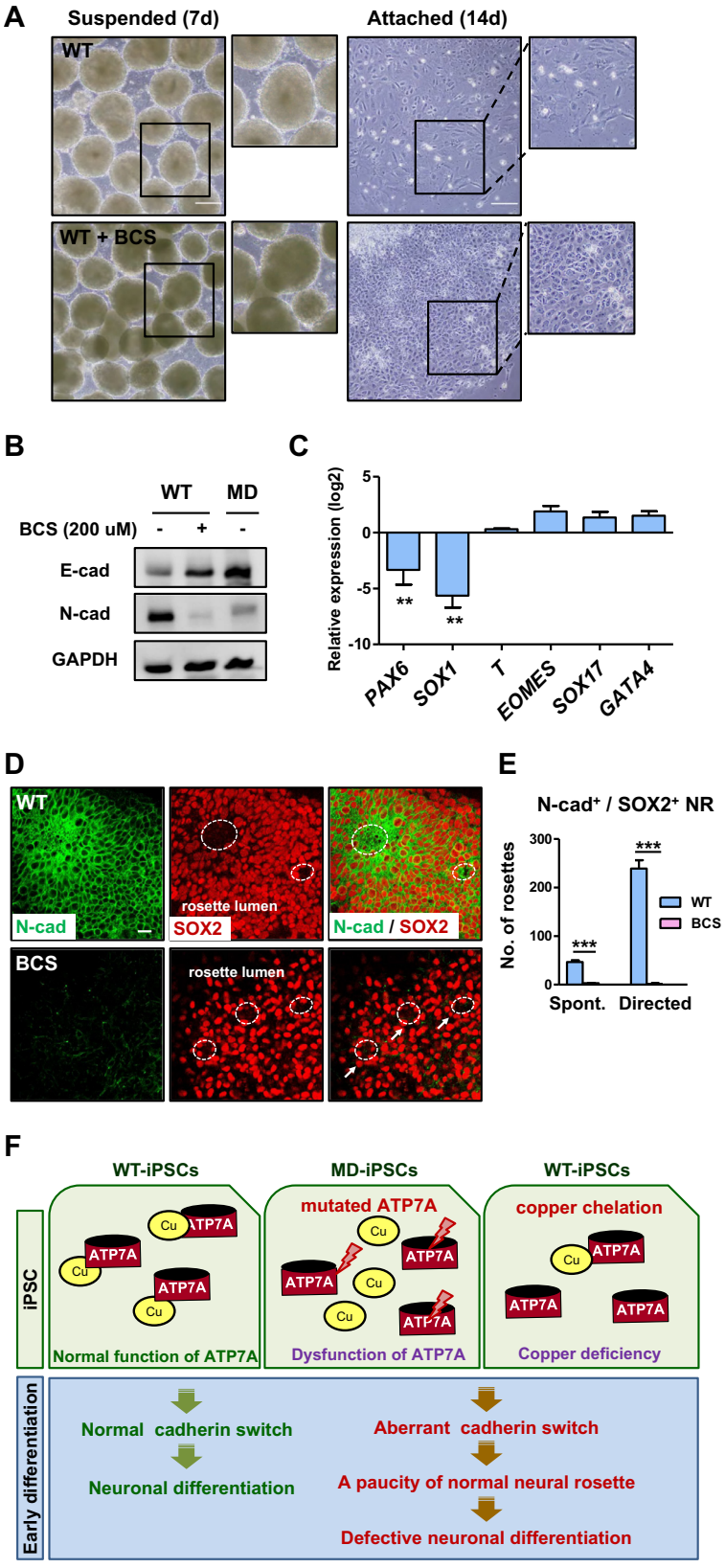

Fig. 4. Effects of copper deficiency on neuronal differentiation of WT-iPSCs. (A) Phase-contrast images. WT-iPSCs were treated with 200 μM bathocuprione sulfate (BCS) during EB development for 7 days (left) and then further cultured on matrigel-coated dishes (right, day 14), respectively. Black squares are magnified images. (B) Western blot analysis of E-cad and N-cad at day 14 during early differentiation in BCS-treated iPSCs. (C) Relative expression level of lineage-specific genes in BCS-treated iPSC-derivatives compared with WT-iPSC-derivatives at 14 day of culture. *p* Values were analyzed by Mann–Whitney test (**$p < 0.01$). (D) Immunostaining of N-cad (green) and SOX2 (red) in BCS-treated neurospheres by using directed neuronal differentiation method. White dot circles represent lumens of neural rosette structure. White arrows indicate empty lumens of rosette structures in BCS-treated neurospheres. (E) Number of N-cad/SOX2 double positive neural rosettes per each well (***$p < 0.001$). All scale bars represent 200 μm. (F) Proposed model for role of ATP7A related with copper in early differentiation. (For interpretation of the references to color in this figure legend, the reader is referred to the web version of this article.)

tures at 7 day of suspension culture compared with WT-iPSC-derivatives (Fig. 2A, left). Attached cells from MD-iPSC-derived EBs had epithelial morphology, unlike WT-iPSC-derivatives (Fig. 2A, right). From these results, it was hypothesized that MD-iPSCs might be impaired in an early differentiation process. To address this question, expression of E-cadherin (E-cad) and N-cadherin (N-cad), which are associated with the commitment of differentiation from a pluripotent state [21], were examined. During *in vitro* differentiation via EB formation, transcriptional levels of *E-cad* were retained in MD-iPSC-derivatives and gradually decreased in WT-iPSC-derivatives. Also, increase of *N-cad* transcripts was not significant in MD-iPSC-derivatives compared to WT-iPSC-derivatives (Fig. 2B). This disparity was also observed at the protein level (Fig. 2C). Cadherin molecules are regulated by various signaling pathways such as EMT pathway and play an important role to maintain the cell-to-cell junction in epithelial cells. To determine whether this abnormal cadherin switch was affected by epithelial–mesenchymal transition (EMT), expression of Snail and Slug was investigated at RNA and protein levels (Supplementary data 2). The results demonstrated no correlation of cadherin switch and EMT in MD-iPSCs during early differentiation. Next, it was investigated whether this cadherin switch failure influences determination of the cell fate. Intriguingly, transcription of neuroectodermal genes *PAX6* and *SOX1* was inactivated in MD-iPSCs during spontaneous differentiation as compared with WT-iPSCs (Fig. 2D). In contrast, transcripts of mesodermal (*T* and *EOMES*) and endodermal genes (*SOX17* and *GATA4*) were enriched in MD-iPSC-derivatives at 14 day of differentiation (Fig. 2E). These results suggest that abnormal switch of E-cad to N-cad may affect the cell fate determination to neuroectodermal lineage during *in vitro* differentiation.

3.3. A paucity of neural rosette formation in MD-iPSCs

MD-iPSCs were differentiated to neurospheres by two methods of spontaneous and directed differentiation (Supplementary data 3). Unlike in WT-iPSCs, N-cad was not expressed in neurospheres spontaneously and directly differentiated from MD-iPSCs (Fig. 3A and B, respectively), thereby resulting in shapes of empty rosette lumens. MD-iPSCs also showed lower expression of NESTIN and aberrant rosette lumens during neurosphere development (Supplementary data 4). In addition, the number of N-cad$^+$/SOX2$^+$ neural rosettes was significantly decreased in MD-iPSCs compared to WT-iPSCs in respective differentiation methods (Fig. 3C). Transcriptional activation of early neuronal genes (*PAX6*, *SOX1*, and *OTX2*) was not induced in MD-iPSCs during directed neuronal differentiation (Fig. 3D). Subsequently, MD-iPSCs could not differentiate into the MAP2- and TUJ-1-expressing neurites (Fig. 3E). Next experiments were performed to examine the differentiation potential of MD-iPSCs into cell types of other developmental lineages such as the mesoderm and endoderm. As results, MD-iPSCs differentiated into smooth muscle cells (Supplementary data 5) and hepatocytes (Supplementary data 6). These results clearly indicate that the aberrant switch of E-cad to N-cad might impair determination of neuronal lineage in the Menkes disease.

3.4. Effects of copper deficiency on neuronal differentiation of WT-iPSCs

To clarify whether the aberrant switch of E-cad to N-cad in MD-iPSCs be due to copper deficiency, WT-iPSCs were treated with a copper chelator, bathocuprione sulfate (BCS), throughout differentiation via EB formation for 14 days. Like MD-iPSC-derivatives, surprisingly, BCS-treated EBs became opaque and compact in appearance and showed epithelial shapes in the attached culture (Fig. 4A). Also, switch of E-cad to N-cad did not occur in BCS-treated EBs during differentiation (Fig. 4B). Like in MD-iPSCs, transcription of neuroectodermal genes (*PAX6* and *SOX1*) were downregulated whereas expression profiles of mesodermal genes (*T* and *EOMES*) and endodermal genes (*SOX17* and *GATA4*) were similar in BCS-treated EBs during differentiation compared with non-treated EBs (Fig. 4C). When WT-iPSCs were treated with a copper chelator during neuronal differentiation, BCS-treated neurospheres did not express N-cad (Fig. 4D), thereby making empty rosette lumens. Number of N-cad$^+$/SOX2$^+$ neural rosettes significantly decreased in BCS-treated samples derived by both differentiation methods (Fig. 4E, $p < 0.001$). mRNA levels of early neuronal marker genes (*PAX6*, *SOX1*, and *OTX2*) were low in BCS-treated samples compared to WT-samples (data not shown). This result indicates that copper is essential for the switch of E-cad to N-cad in human iPSCs during neural differentiation. Thus, we found that copper chelation gave rise to the aberrant cadherin switch and impaired neural rosette formation in WT-iPSCs during early differentiation, recapitulating *in vitro* phenotypes of MD-iPSCs. These results suggest that dysfunction of ATP7A and/or copper deficiency lead to aberrant cadherin switch, eventually resulting in defective early neuronal development in Menkes disease.

4. Discussion

Here, we demonstrate for the first time aberrant molecular and cellular phenotypes in terms of the cadherin switch and neural rosette formation in MD-iPSCs during neuronal differentiation. The cadherin switch is known to play critical roles in normal embryonic development and organogenesis [22]. A transition of E-cad to N-cad occurs in hESCs during spontaneous differentiation [21]. But, MD-iPSCs exhibited abnormal cadherin switch at the transcriptional and protein levels during early differentiation (Fig. 2). Furthermore, this aberrant cadherin switch in MD-iPSCs directly impaired neural rosette formation (Fig. 3), indicating the importance of the cadherin switch in the early neuronal differentiation. Decreased number of neuronal cells and disrupted organization of neurons were observed at early post-natal stage in ATP7A knockout mice [13]. Therefore, our findings suggest that an abnormal cadherin switch may give rise to neurological defects in Menkes disease patients. In many Menkes disease infants, it has been reported that activities of copper-requiring enzymes such as dopamine-β-hydroxlyase and peptidyl-glycine-α-amidating monooxygenase, which are closely related with neurologic pathologies, are reduced [10,23]. Here, we could not measure the activity of copper-requiring enzymes because MD-iPSCs did not differentiate into neuronal cells. Like MD-iPSCs, copper-chelated WT-iPSCs showed aberrant cadherin switch and impaired neuronal differentiation during early differentiation (Fig. 4). These results imply that copper is an essential element for normal cadherin switch in early neuronal development.

This study may provide new insights to understand strategies to treat Menkes disease. Even though the treatment of choice for Menkes disease, currently copper–histidine replacement therapy, has relieved neurologic complications in some patients, the effect of the treatment on survival rate or long term neurologic morbidity is inconclusive. A limitations of the copper treatment in Menkes disease is thought to be due to blood–brain and blood–cerebrospinal fluid barriers [16,24]. Although copper concentration level of MD-iPSCs was similar to that of WT-iPSCs (Table 2), in this study, MD-iPSCs showed aberrancies in the early neuronal differentiation (Fig. 3). A paper reported that copper level of MD-fibroblasts was increased in physiologic culture condition [25]. Although intracellular location or delivery mechanism of excessive coppers in MD-fibroblasts remains obscure [26], abnormal distribution of ATP7A moelcules was observed in MD-fibroblasts and MD-iPSCs

(Fig. 1E). From these results, it is likely that mutated ATP7A may reduce intracellular utilization of copper molecules. Also, copper chelation in WT-iPSCs resembled defective phenotypes of MD-iPSCs during early neuronal differentiation. As a model, either copper deficiency or dysfunction of ATP7A may impair neuronal development in Menkes disease (Fig. 4F).

Aberrant cadherin transition and abnormal neural rosette formation in MD-iPSCs observed in this study can explain severe neurologic phenotypes that are poorly understood in Menkes disease patients. Defects of early neuronal differentiation in MD-iPSCs indirectly support that initial onset of Menkes disease may begin from early neuronal development. In conclusion, this study provides a possible mechanism that can explain neurologic symptoms in Menkes disease, especially in early neuronal development.

Acknowledgments

We sincerely thank Younghee Ju and Kyu-Min Han for their efforts to maintain hiPSCs and Prof. Seyun Kim for valuable discussion. This research was supported by a Grant (A084697) from the Korea Healthcare Technology R&D project funded by Ministry of Health and Welfare, Republic of Korea.

Appendix A. Supplementary data

Supplementary data associated with this article can be found, in the online version, at http://dx.doi.org/10.1016/j.bbrc.2014.01.038.

References

[1] S.G. Kaler, ATP7A-related copper transport diseases-emerging concepts and future trends, Nat. Rev. Neurol. 7 (2011) 15–29.
[2] J.H. Menkes, M. Alter, G.K. Steigleder, D.R. Weakley, J.H. Sung, A sex-linked recessive disorder with retardation of growth, peculiar hair, and focal cerebral and cerebellar degeneration, Pediatrics 29 (1962) 764–779.
[3] D.J. Waggoner, T.B. Bartnikas, J.D. Gitlin, The role of copper in neurodegenerative disease, Neurobiol. Dis. 6 (1999) 221–230.
[4] J. Chelly, Z. Tumer, T. Tonnesen, A. Petterson, Y. Ishikawa-Brush, N. Tommerup, N. Horn, A.P. Monaco, Isolation of a candidate gene for Menkes disease that encodes a potential heavy metal binding protein, Nat. Genet. 3 (1993) 14–19.
[5] J.F. Mercer, J. Livingston, B. Hall, J.A. Paynter, C. Begy, S. Chandrasekharappa, P. Lockhart, A. Grimes, M. Bhave, D. Siemieniak, et al., Isolation of a partial candidate gene for Menkes disease by positional cloning, Nat. Genet. 3 (1993) 20–25.
[6] C. Vulpe, B. Levinson, S. Whitney, S. Packman, J. Gitschier, Isolation of a candidate gene for Menkes disease and evidence that it encodes a copper-transporting ATPase, Nat. Genet. 3 (1993) 7–13.
[7] B.E. Kim, K. Smith, C.K. Meagher, M.J. Petris, A conditional mutation affecting localization of the Menkes disease copper ATPase. Suppression by copper supplementation, J. Biol. Chem. 277 (2002) 44079–44084.
[8] M.J. Petris, I. Voskoboinik, M. Cater, K. Smith, B.E. Kim, R.M. Llanos, D. Strausak, J. Camakaris, J.F. Mercer, Copper-regulated trafficking of the Menkes disease copper ATPase is associated with formation of a phosphorylated catalytic intermediate, J. Biol. Chem. 277 (2002) 46736–46742.
[9] S.G. Kaler, Menkes disease, Adv. Pediatr. 41 (1994) 263–304.
[10] S.G. Kaler, C.S. Holmes, D.S. Goldstein, J. Tang, S.C. Godwin, A. Donsante, C.J. Liew, S. Sato, N. Patronas, Neonatal diagnosis and treatment of Menkes disease, N. Engl. J. Med. 358 (2008) 605–614.
[11] J. Christodoulou, D.M. Danks, B. Sarkar, K.E. Baerlocher, R. Casey, N. Horn, Z. Tumer, J.T. Clarke, Early treatment of Menkes disease with parenteral copper-histidine: long-term follow-up of four treated patients, Am. J. Med. Genet. 76 (1998) 154–164.
[12] J. Kreuder, A. Otten, H. Fuder, Z. Tumer, T. Tonnesen, N. Horn, D. Dralle, Clinical and biochemical consequences of copper–histidine therapy in Menkes disease, Eur. J. Pediatr. 152 (1993) 828–832.
[13] R. El Meskini, K.L. Crabtree, L.B. Cline, R.E. Mains, B.A. Eipper, G.V. Ronnett, ATP7A (Menkes protein) functions in axonal targeting and synaptogenesis, Mol. Cell. Neurosci. 34 (2007) 409–421.
[14] Y. Mototani, I. Miyoshi, T. Okamura, T. Moriya, Y. Meng, X. Yuan Pei, S. Kameo, N. Kasai, Phenotypic and genetic characterization of the Atp7a(Mo-Tohm) mottled mouse: a new murine model of Menkes disease, Genomics 87 (2006) 191–199.
[15] M.J. Niciu, X.M. Ma, R. El Meskini, G.V. Ronnett, R.E. Mains, B.A. Eipper, Developmental changes in the expression of ATP7A during a critical period in postnatal neurodevelopment, Neuroscience 139 (2006) 947–964.
[16] P.C. Liu, Y.W. Chen, J.A. Centeno, M. Quezado, K. Lem, S.G. Kaler, Downregulation of myelination, energy, and translational genes in Menkes disease brain, Mol. Genet. Metab. 85 (2005) 291–300.
[17] M.C. Marchetto, B. Winner, F.H. Gage, Pluripotent stem cells in neurodegenerative and neurodevelopmental diseases, Hum. Mol. Genet. 19 (2010) R71–R76.
[18] A.R. Muotri, Modeling epilepsy with pluripotent human cells, Epilepsy Behav. 14 (Suppl. 1) (2009) 81–85.
[19] S.H. Ahn, S.Y. Park, S.G. Kang, J.E. Lee, Y.S. Kwon, B.K. Son, H.W. Yoo, A case of Menkes disease with infantile spasm, J. Korean Child Neurol. Soc. 15 (2007) 199–204.
[20] K. Takahashi, K. Tanabe, M. Ohnuki, M. Narita, T. Ichisaka, K. Tomoda, S. Yamanaka, Induction of pluripotent stem cells from adult human fibroblasts by defined factors, Cell 131 (2007) 861–872.
[21] A.M. Eastham, H. Spencer, F. Soncin, S. Ritson, C.L. Merry, P.L. Stern, C.M. Ward, Epithelial–mesenchymal transition events during human embryonic stem cell differentiation, Cancer Res. 67 (2007) 11254–11262.
[22] H. Acloque, M.S. Adams, K. Fishwick, M. Bronner-Fraser, M.A. Nieto, Epithelial–mesenchymal transitions: the importance of changing cell state in development and disease, J. Clin. Invest. 119 (2009) 1438–1449.
[23] S.G. Kaler, C.J. Liew, A. Donsante, J.D. Hicks, S. Sato, J.C. Greenfield, Molecular correlates of epilepsy in early diagnosed and treated Menkes disease, J. Inherit. Metab. Dis. 33 (2010) 583–589.
[24] A. Donsante, P. Johnson, L.A. Jansen, S.G. Kaler, Somatic mosaicism in Menkes disease suggests choroid plexus-mediated copper transport to the developing brain, Am. J. Med. Genet. A 152A (2010) 2529–2534.
[25] T.J. Goka, R.E. Stevenson, P.M. Hefferan, R.R. Howell, Menkes disease: a biochemical abnormality in cultured human fibroblasts, Proc. Natl. Acad. Sci. USA 73 (1976) 604–606.
[26] B.E. Kim, T. Nevitt, D.J. Thiele, Mechanisms for copper acquisition, distribution and regulation, Nat. Chem. Biol. 4 (2008) 176–185.